



HAL
open science

Foliar uptake of atmospheric nitrate by two dominant subalpine plants: insights from in situ triple-isotope analysis

Ilann Bourgeois, Jean-Christophe Clement, Nicolas Caillon, Joel Savarino

► To cite this version:

Ilann Bourgeois, Jean-Christophe Clement, Nicolas Caillon, Joel Savarino. Foliar uptake of atmospheric nitrate by two dominant subalpine plants: insights from in situ triple-isotope analysis. *New Phytologist*, 2019, 223 (4), pp.1784-1794. 10.1111/nph.15761 . hal-02350376

HAL Id: hal-02350376

<https://hal.science/hal-02350376>

Submitted on 26 Nov 2020

HAL is a multi-disciplinary open access archive for the deposit and dissemination of scientific research documents, whether they are published or not. The documents may come from teaching and research institutions in France or abroad, or from public or private research centers.

L'archive ouverte pluridisciplinaire **HAL**, est destinée au dépôt et à la diffusion de documents scientifiques de niveau recherche, publiés ou non, émanant des établissements d'enseignement et de recherche français ou étrangers, des laboratoires publics ou privés.

DR ILANN BOURGEOIS (Orcid ID : 0000-0002-2875-1258)

DR JEAN-CHRISTOPHE CLEMENT (Orcid ID : 0000-0002-0841-7199)

Article type : Regular Manuscript

Foliar uptake of atmospheric nitrate by two dominant subalpine plants: insights from *in situ* triple-isotope analysis

Ilann Bourgeois^{1,2,*,\$}, *Jean-Christophe Clément*^{2,3}, *Nicolas Caillon*¹ and *Joël Savarino*¹

¹Univ. Grenoble Alpes, CNRS, IRD, Grenoble INP, IGE, F-38000, Grenoble, France

²Univ. Grenoble Alpes, CNRS, LECA, F-38000, Grenoble, France

³Univ. Savoie Mont Blanc, INRA, CARRTEL, F-74200, Thonon-Les Bains, France

^{\$}Now at

Cooperative Institute for Research in Environmental Sciences, University of Colorado Boulder,
Boulder, Colorado, USA.

NOAA Earth System Research Laboratory, Boulder, Colorado, USA.

This article has been accepted for publication and undergone full peer review but has not been through the copyediting, typesetting, pagination and proofreading process, which may lead to differences between this version and the Version of Record. Please cite this article as doi: 10.1111/nph.15761

This article is protected by copyright. All rights reserved.

*Corresponding author: ilann.bourgeois@noaa.gov / +1-303-497-6302

Received: 23 October 2018

Accepted: 19 February 2019

ORCID: I. Bourgeois (0000-0002-2875-1258), J.-C. Clément (0000-0002-0841-7199), N. Caillon (0000-0002-6318-6194), J. Savarino (0000-0002-6708-9623).

Summary

- The significance of foliar uptake of nitrogen (N) compounds in natural conditions is not well understood, despite growing evidence of its importance to plant nutrition. In subalpine meadows, N-limitation fosters the dominance of specific subalpine plant species, which in turn ensure the provision of essential ecosystems services. Understanding how these plants absorb N and from which sources is important to predict ecological consequences of increasing N deposition.
- Here, we investigate the sources of N to plants from subalpine meadows with distinct land-use history in the French Alps, using the triple isotopes ($\Delta^{17}\text{O}$, $\delta^{18}\text{O}$, and $\delta^{15}\text{N}$) of plant tissue nitrate (NO_3^-). We use this approach to evaluate the significance of foliar uptake of atmospheric NO_3^- ($\text{NO}_3^-_{\text{atm}}$).
- The foliar uptake of $\text{NO}_3^-_{\text{atm}}$ accounted for 4-16 % of the leaf NO_3^- content, and contributed more to the leaf NO_3^- pool after peak biomass. Additionally, the gradual ^{15}N enrichment of NO_3^- from the soil to the leaves reflected the contribution of $\text{NO}_3^-_{\text{atm}}$ assimilation to plants' metabolism.
- The present study confirms that foliar uptake is a potentially important pathway for $\text{NO}_3^-_{\text{atm}}$ into subalpine plants. This is of major significance as N emissions (and deposition) are predicted to increase globally in the future.

This article is protected by copyright. All rights reserved.

Keywords

Subalpine plants, atmospheric nitrate, stable isotopes, foliar uptake, nitrogen deposition

Introduction

Monitoring atmospheric nitrogen (N) deposition has greatly improved our understanding of the effects of anthropogenic changes on the environment (Vitousek *et al.*, 1997; Galloway *et al.*, 2008; Fowler *et al.*, 2015). Human activities (e.g., fossil fuel combustion and agriculture) have led to increased emissions of reactive nitrogen species ($N_r = NO_y, NH_x$), which in turn have increased inputs of N to the environment worldwide (Galloway *et al.*, 2004; Cui *et al.*, 2013). Some consequences of this altered N cycle include soil acidification, biodiversity loss, intensified N leaching, eutrophication, and public health issues (Aber *et al.*, 1989; Galloway *et al.*, 2003; Ward *et al.*, 2005; Clark *et al.*, 2013).

Mountain regions are particularly vulnerable to changes in the N cycle: their shallow soils have a low acidification buffering capacity, while the endemic plants have developed N uptake strategies that are optimized for low nutrient environments (Bowman *et al.*, 2006; Bassin *et al.*, 2013; Boutin *et al.*, 2017). For example, intermediate stages of N saturation (Aber *et al.*, 1989) have been measured in elevated sites in the Colorado Front Range, USA (Williams & Tonnessen, 2000; Burns, 2004; Baron, 2006), as a result of regionally elevated N deposition (Mladenov *et al.*, 2012; Clow *et al.*, 2015; Nanus *et al.*, 2018).

In high altitude catchments, the N balance is still poorly understood. The fraction of atmospheric N efficiently retained or lost, and where and how this occurs, remains unknown. While deposition of atmospheric N often exceeds losses to streams *via* leaching and runoff (Baron & Campbell, 1997; Mast *et al.*, 2014), the respective importance of potential N sinks (e.g., microbial and abiotic immobilization, plant uptake, denitrification) is not yet constrained (Weintraub *et al.*, 2017). In addition, atmospheric N dynamics in the mountainous soil/plant continuum are inextricably linked to the complex topography and hydrology of these ecosystems (Balestrini *et al.*, 2013; Weintraub *et al.*,

2017; Bourgeois *et al.*, 2018b). While assessing the fate of deposited N in high altitude catchments is complex, it is necessary to understand nutrient partitioning in these essential ecosystems to preserve freshwater quality, erosion control and their patrimonial value (Clément *et al.*, 2012; Thébault *et al.*, 2014).

Several studies have established that reactive atmospheric N species (e.g., NO₂, HNO₃, and NH₃) may be incorporated directly into plant leaves and used as a nutritional source (Vallano & Sparks, 2007 and literature therein). In N-limited soils, N availability to plants largely depends on competing or loss processes such as microbial immobilization (Kaye & Hart, 1997) and leaching (Hood *et al.*, 2003). Foliar uptake can provide an alternative N absorption pathway to plants, and its significance needs to be evaluated to better predict how these N-poor ecosystems will respond to a globally increasing N deposition (Fowler *et al.*, 2013). However, an accurate parameterization of this mechanism is absent from most ecological models (Sparks, 2009). To our knowledge, no study has quantified the magnitude of foliar uptake *in situ* (*i.e.*, under natural atmospheric N deposition rates). Most estimates of foliar uptake are reported as contributing 0-50% of plant N demand (Sparks, 2009 and literature therein). Yet, these studies were either conducted at the individual plant scale, in the laboratory (*i.e.*, unnatural conditions), or at the ecosystem scale, using imperfect throughfall measurements. An accurate partitioning of N absorption pathways (root *vs.* foliar) will be key to predicting the impact of increasing atmospheric N deposition on ecosystem productivity.

The dual isotopes ($\delta^{18}\text{O}$ and $\delta^{15}\text{N}$) of nitrate (NO₃⁻) have provided a refined understanding of the N cycle across a variety of terrestrial and aquatic ecosystems (Durka *et al.*, 1994; Mayer *et al.*, 2002; Wankel *et al.*, 2006; Nanus *et al.*, 2008; Hastings *et al.*, 2009). Kendall *et al.* (2007) characterized the $\delta^{18}\text{O}$ and $\delta^{15}\text{N}$ ranges of NO₃⁻ from different sources (e.g., nitrification, atmospheric deposition), from which the origin of NO₃⁻ in a given environmental pool can be determined. However, terrestrial reservoirs of NO₃⁻ and NH₄⁺ can undergo a large variety of physical, chemical or biological processes (e.g., mineralization, nitrification, assimilation, volatilization) that impact their isotopic composition, also called fractionation. During the nitrification process, the newly produced NO₃⁻ is ¹⁵N-depleted compared to the residual NH₄⁺ pool (Mariotti *et al.*, 1981). During the denitrification and biological

This article is protected by copyright. All rights reserved.

assimilation processes, the residual NO_3^- pools are ^{15}N - and ^{18}O -enriched (Mariotti *et al.*, 1981, 1982; Granger *et al.*, 2004, 2010). Although some of these isotopic effects were successfully characterized, understanding the complex dynamics of the N cycle based on $\delta^{18}\text{O}$ and $\delta^{15}\text{N}$ of NO_3^- is not straightforward. Pioneering studies successfully used the dual isotope approach to evaluate the sources of NO_3^- in moss tissues (Liu *et al.*, 2012b,a, 2013c,a). However, the interpretation of $\delta^{18}\text{O}$ and $\delta^{15}\text{N}$ values of NO_3^- (referred to as $\delta^{18}\text{O}\text{-NO}_3^-$ and $\delta^{15}\text{N}\text{-NO}_3^-$ in this paper) is much more challenging in vascular plants due to the simultaneous effects of source mixing and biological isotope fractionation and their impacts on plant tissue NO_3^- isotopes (Liu *et al.*, 2013b, 2014). Recently, the triple isotope ($\Delta^{17}\text{O}$, $\delta^{18}\text{O}$, and $\delta^{15}\text{N}$) composition of NO_3^- has been proposed as a more robust tool to identify NO_3^- sources and infer the biological underlying processes driving the N cycle (Michalski *et al.*, 2004; Costa *et al.*, 2011). Atmospheric NO_3^- ($\text{NO}_3^-_{\text{atm}}$) is characterized by a high $\Delta^{17}\text{O}$ value ranging from 20 to 35‰ (Savarino *et al.*, 2013), whereas biologically-derived NO_3^- ($\text{NO}_3^-_{\text{bio}}$) exhibits a $\Delta^{17}\text{O}$ value of 0‰ (Michalski *et al.*, 2004). The contribution of $\text{NO}_3^-_{\text{atm}}$ can thus be quantified through a simple two end-member mixing model. This triple isotopic tracer of NO_3^- unequivocally reveals direct $\text{NO}_3^-_{\text{atm}}$ inputs in environmental pools, and provides a better assessment of biologically-induced fractionation of NO_3^- isotopes compared to the traditional dual isotope technique (Rose *et al.*, 2015; Fang *et al.*, 2015). The triple isotopic tracer method has for instance recently been used to monitor $\text{NO}_3^-_{\text{atm}}$ uptake and assimilation by forests and tundra across a variety of ecosystems (Liu *et al.*, 2018).

Here, we tested two main hypotheses: i) NO_3^- triple isotopes can be used to quantify the proportion of $\text{NO}_3^-_{\text{atm}}$ in the nitrate pool of subalpine plant tissues, and ii) NO_3^- triple isotopes can be used to evaluate the significance of foliar N uptake and track its seasonal variability. To verify these hypotheses, we measured the concentration and triple isotopic composition ($\Delta^{17}\text{O}$, $\delta^{18}\text{O}$, and $\delta^{15}\text{N}$) of NO_3^- , along with the concentration of ammonium (NH_4^+), in precipitation, soils, and different tissues (roots and leaves) of two dominant subalpine plant species at the Lautaret pass in the central French Alps. We also tested the question of land-use influence on foliar uptake of N. The vegetation at the Lautaret pass is dominated by grassland communities whose diversity and functional traits depend on

past (terraced *vs.* unterraced) and current (mowing, grazing) land use (Quétier *et al.*, 2007). These distinct land-use trajectories have been shown to deeply impact the N turnover rates in subalpine soils (Robson *et al.*, 2007, 2010; Legay *et al.*, 2013), mostly because of differences in N availability, microbial communities and abiotic parameters (Legay *et al.*, 2016). Here, we hypothesized that foliar uptake of $\text{NO}_3^-_{\text{am}}$ would contribute in larger proportion to plant N nutrition in less fertile grasslands with low N availability.

Material & Methods

Site Description

The Lautaret and Les Cours sub-watersheds are located in the upper Romanche valley of the central French Alps, near the Lautaret pass (45°02'N; 6°20'E, 1650-2000 m a.s.l., Figure S1). The site forms part of the French National Research Infrastructure to study continental ecosystems and their biodiversity (AnaEE – France, <https://www.anaee-france.fr>) and of the Long-Term Ecological Research network (LTER, <https://www.ilter.network>). The Lautaret pass is characterized by a seasonal snow-cover (November to April) and a short vegetative period (May to September, hereafter denoted as “annual”). Temperatures averaged -3.0°C and 13.0°C in January and August 2016, respectively, while multi-year (2004-2010) means were -6.5°C and 13.9°C. The annual cumulative precipitation was 609 mm, significantly lower than the multi-year (2004-2010) mean of 956 mm.

Here, we consider three grasslands featuring three combinations of past (terraced *vs.* unterraced) and present (mown *vs.* unmown) land uses (Quétier *et al.*, 2007). Two grasslands are situated on the terraced slopes of Les Cours watershed (Figure S1); one is mown for hay in August and grazed in autumn (terraced and mown, TM) while the other is not mown but grazed in summer (terraced and unmown, TU). The third grassland is located on the Lautaret watershed (Figure S1) and is unterraced, never mown (unterraced and unmown, UU) and only very lightly grazed in summer. The management practices in the study area remained unchanged since at least 2003, which led to substantial

Accepted Article

differences in plant communities and soil properties between each grassland (Legay *et al.*, 2013). Generally, the terraced meadows were dominated by species showing exploitative traits (higher specific leaf area and leaf nitrogen content; Quétier *et al.*, 2007) such as *Dactylis glomerata*, whereas unterraced grasslands were dominated by conservative species (higher internal N recycling; Quétier *et al.*, 2007) like *Festuca paniculata*. These two species have very different functional traits, N uptake strategies, and competition levels with soil microbial biomass (Robson *et al.*, 2010; Legay *et al.*, 2013).

Samples collection and analysis

To account for spatial variability, each grassland was subdivided into three plots to provide three plant samples per grassland. A total of 9 individual plants were thus collected per sampling date (3 grasslands \times 3 individual plants). Between May and September 2016, we harvested either one tuft of *D. glomerata* or of *F. paniculata* from each subplot (including several tillers and the roots) depending on which species dominated the meadow. At the same time, we collected cylindrical soil cores (4.5 cm in diameter and 8 cm in length) from the same locations. Sampling was performed twice a month around midday until peak biomass was reached (from May to July), and continued on a monthly basis afterward (July through September). Potential diurnal variations of inorganic N (NO_3^- , NH_4^+) concentrations in plants were not investigated. From April to October 2016, separate samples for wet and dry deposition were collected every three weeks using an atmospheric deposition collector (WADOS Kroneis GmbH, Austria). Precipitation samples were kept frozen until further chemical analysis. The dry deposition funnel was rinsed with 500 mL of ultrapure water ($18.2 \text{ M}\Omega\cdot\text{cm}^{-1}$) and the sample stored at -20°C .

All plants were thoroughly washed with ultrapure water. Aerial parts (*i.e.*, leaves, shoots, and stems) were then separated from those below ground (*i.e.*, roots), and then frozen. Leaves, shoots, and stems were combined and collectively referred to as “leaves” hereafter. Samples were later freeze-dried (Heto DryWinner, Allerød, Denmark), ground to powder (RETSCH Mixer Mill MM400), and

Accepted Article

homogenized. Dissolved inorganic nitrogen (DIN) was extracted by shaking (300 RPM for 1h) 1.0 g (*D. glomerata*) and 1.5 g (*F. paniculata*) dry weight (dw) of powdered leaf and root tissues in 50 mL of ultrapure water. Soils were passed through a 2 mm sieve to remove rocks and roots. Subsamples of sieved soils (10.0 g dw) were shaken (300 RPM for 1h) in 50 mL of ultrapure water to extract the DIN. After centrifugation (4000 RPM for 10 min), all plant and soil samples were filtered using 0.22 μm quartz filters (QMA Whatman). Precipitation samples were left to melt at ambient temperature and filtered using 0.45 μm quartz filters (QMA Whatman).

All samples were subsequently analyzed for concentrations of NH_4^+ , NO_3^- , and NO_2^- (the latter being always negligible compared to $[\text{NO}_3^-]$) using a colorimetric technique (Gallery Plus, Thermo Fisher Scientific, Waltham, Massachusetts, USA). The analytical error of $\pm 0.01 \text{ mg L}^{-1}$ was determined from the standard deviation of commercial control solutions (ThermoFisher[®]). Isotopic analyses were conducted on a MAT 253 IRMS using an adapted version of the denitrifier method (Kaiser *et al.*, 2007; Morin *et al.*, 2008). The analytical errors – calculated as the standard deviation of the residuals from the linear regression between raw data of the reference standards (USGS 32, USGS 34 and USGS 35) and their accepted values – were ± 0.5 , 2.1, and 0.3 ‰ for $\Delta^{17}\text{O}$, $\delta^{18}\text{O}$, and $\delta^{15}\text{N}$ of NO_3^- , respectively. Slopes and intercepts of the linear regressions were then used to convert raw sample data into calibrated values (VSMOW scale for O isotopes, and N_2 -air scale for N isotopes).

Isotopic end-member mixing model

While the oxygen isotopic composition of $\text{NO}_3^-_{bio}$ follows the mass-dependent law $\delta^{17}\text{O} \approx 0.52 \times \delta^{18}\text{O}$ (Miller, 2002), that of $\text{NO}_3^-_{am}$ differs as its production pathway involves O_3 , containing an excess of ^{17}O of 25-35 ‰ (Vicars & Savarino, 2014). As a result, ^{17}O excess (denoted by $\Delta^{17}\text{O}$, with $\Delta^{17}\text{O} = \delta^{17}\text{O} - 0.52 \times \delta^{18}\text{O}$) of $\text{NO}_3^-_{am}$ ranges from 20 to 35 ‰ (Savarino *et al.*, 2013), whereas NO_3^- from other sources has a $\Delta^{17}\text{O}$ of zero (Michalski *et al.*, 2004). In this study, a simple mixing model was used to quantify the unprocessed $\text{NO}_3^-_{am}$ fraction (f_{am}) in samples, according to Michalski *et al.* (2004):

(Eq.1)
$$f_{atm} = \Delta^{17}\text{O-NO}_3^-_{sample} / \Delta^{17}\text{O-NO}_3^-_{atm}$$

We used a value of $\Delta^{17}\text{O-NO}_3^-_{atm} = 24.4 \pm 2.4 \text{ ‰}$, corresponding to the mean concentration-weighted value of $\Delta^{17}\text{O-NO}_3^-$ found in wet and dry deposition samples collected during the study (Table 1).

To our knowledge, there are two possible sources of $\text{NO}_3^-_{atm}$ in leaves. One is the direct leaf uptake via stomata or cuticles, and the other is the translocation of deposited $\text{NO}_3^-_{atm}$ from soil to roots, and then to the leaves. Therefore, we used the following isotope mass-balance approach to estimate the foliar absorption of $\text{NO}_3^-_{atm}$:

(Eq.2)
$$\Delta^{17}\text{O-NO}_3^-_{leaf} = \Delta^{17}\text{O-NO}_3^-_{atm} * f_{uptake} + \Delta^{17}\text{O-NO}_3^-_{root} * f_{translocation}$$

(Eq.3)
$$f_{uptake} + f_{translocation} = 1$$

Where f_{uptake} and $f_{translocation}$ are the fractions of atmospheric $\text{NO}_3^-_{atm}$ out of the leaf NO_3^- pool from foliar uptake and translocation, respectively. After substituting Eq.3 into Eq.2, we get:

(Eq.4)
$$f_{uptake} = (\Delta^{17}\text{O-NO}_3^-_{leaf} - \Delta^{17}\text{O-NO}_3^-_{root}) / (\Delta^{17}\text{O-NO}_3^-_{atm} - \Delta^{17}\text{O-NO}_3^-_{root})$$

Data correction for atmospheric influence

Mole fractions of NO_3^- (f_{atm} and $f_{bio} = 1 - f_{atm}$) can be used to remove the isotopic influence of $\text{NO}_3^-_{atm}$ on $\text{NO}_3^-_{sample}$ (with $\text{NO}_3^-_{sample} = \text{NO}_3^-_{atm} + \text{NO}_3^-_{bio}$), which allows for a better interpretation of

This article is protected by copyright. All rights reserved.

biological processes that affect its $\delta^{15}\text{N}$ and $\delta^{18}\text{O}$ values (Tsunogai *et al.*, 2010; Dejawakh *et al.*, 2012; Riha *et al.*, 2014):

$$\text{(Eq.5)} \quad \delta^{18}\text{O}_{bio} = (\delta^{18}\text{O}_{sample} - \delta^{18}\text{O}_{atm} * f_{atm}) / f_{bio}$$

$$\text{(Eq.6)} \quad \delta^{15}\text{N}_{bio} = (\delta^{15}\text{N}_{sample} - \delta^{15}\text{N}_{atm} * f_{atm}) / f_{bio}$$

where $\delta^{15}\text{N}_{atm} = -6.0 \pm 4.1$ and $\delta^{18}\text{O}_{atm} = 66.6 \pm 5.8 \text{ ‰}$ were inferred from the mean concentration-weighted NO_3^- isotopes in wet and dry deposition samples collected during the study (Table 1).

Statistical analysis

All statistical analyses were conducted using the R software (v3.2.3). A Mann-Whitney test was applied to determine significant differences of mean concentrations and isotopic values of NO_3^- and NH_4^+ between plant tissues and species, on an annual (Figure 1) or seasonal (Figure 2) basis.

Differences and correlations were considered significant for $p < 0.05$.

Results

Atmospheric N deposition

Mean and associated standard deviation of $\Delta^{17}\text{O}-\text{NO}_3^-$ in wet and dry deposition from May to September 2016 were 23.6 ± 2.0 and $25.1 \pm 2.7 \text{ ‰}$, respectively (Table 1). These values are in the same range as previously reported data for $\Delta^{17}\text{O}-\text{NO}_3^-_{atm}$ (Michalski *et al.*, 2004; Tsunogai *et al.*, 2010, 2016; Costa *et al.*, 2011). The weighted mean $\Delta^{17}\text{O}$ value for total deposition (wet + dry) was $24.4 \pm 2.4 \text{ ‰}$ (Table 1), and was used to quantify the atmospheric component of NO_3^- pools in plants

This article is protected by copyright. All rights reserved.

(see *Material & Methods*, Eq. 1). Mean annual total $\delta^{18}\text{O}-\text{NO}_3^-$ ($66.6 \pm 5.8 \text{‰}$) and $\delta^{15}\text{N}-\text{NO}_3^-$ ($-6.0 \pm 4.1 \text{‰}$) were also consistent with a reservoir of exclusively NO_3^- (Kendall *et al.*, 2007), and these values were used to correct samples from their atmospheric $\delta^{18}\text{O}$ and $\delta^{15}\text{N}$ components (see *Material & Methods*, Eqs. 5 and 6). Based on these data, the calculated magnitude of the annual NO_3^- deposition flux was 3-5 $\text{kg.N}-\text{NO}_3^- \cdot \text{ha}^{-1} \cdot \text{yr}^{-1}$ (Bourgeois *et al.*, personal communication), higher than the N critical load for subalpine ecosystems estimated to be 1-4 $\text{kg.N} \cdot \text{ha}^{-1} \cdot \text{yr}^{-1}$ (Baron *et al.*, 2011; Nanus *et al.*, 2017).

Soil inorganic N pools

N availability in soils differed in the three meadows. Soil NO_3^- concentration in the UU meadow ($14.6 \pm 19.0 \mu\text{g} \cdot \text{g}^{-1} \text{ dw}$) was significantly lower than in the terraced meadows (58.9 ± 46.9 and $52.3 \pm 48.7 \mu\text{g} \cdot \text{g}^{-1} \text{ dw}$ in TU and TM, respectively; Table 2). Soil NH_4^+ concentration was higher in the unmown meadows ($13.0 \pm 13.7 \mu\text{g} \cdot \text{g}^{-1} \text{ dw}$ in UU and $17.5 \pm 29.9 \mu\text{g} \cdot \text{g}^{-1} \text{ dw}$ in TU) compared to the mown one (6.2 ± 4.0 in TM), although not significantly. The ratio $\text{NO}_3^-/\text{NH}_4^+$ was significantly lower in the UU meadow. These results were in line with previous studies at the same site.

Mean and associated standard deviation of $\Delta^{17}\text{O}-\text{NO}_3^-$ in soils were low, and significantly higher in the UU meadow ($0.9 \pm 0.6 \text{‰}$) than in the terraced ones (0.5 ± 0.8 and $0.3 \pm 0.4 \text{‰}$ in TU and TM, respectively; Table 2). While no significant difference was observed in NO_3^- isotopic values between the TU and TM meadows ($\delta^{18}\text{O}-\text{NO}_3^- = -10.3 \pm 6.6$ and $-10.9 \pm 5.1 \text{‰}$, and $\delta^{15}\text{N}-\text{NO}_3^- = -1.3 \pm 9.6$ and $-2.6 \pm 6.5 \text{‰}$, respectively), $\delta^{18}\text{O}-\text{NO}_3^-$ and $\delta^{15}\text{N}-\text{NO}_3^-$ were significantly higher ($-4.3 \pm 6.8 \text{‰}$) and lower ($-5.1 \pm 6.6 \text{‰}$), respectively, in the UU meadow.

Plant inorganic N pools

The mean $[\text{NO}_3^-]$ in plant tissues varied between 10.0 ± 5.4 and $38.8 \pm 50.8 \mu\text{g} \cdot \text{g}^{-1} \text{ dw}$, and no significant difference was found between plant species or between plant tissues, except for *D*.

This article is protected by copyright. All rights reserved.

glomerata in TU fields (Figure 1a). This range of $[\text{NO}_3^-]$ is similar to the 6-60 $\mu\text{g}\cdot\text{g}^{-1}$ dw range in Arctic vegetation where N is limited (Liu *et al.*, 2018). The mean $[\text{NH}_4^+]$ in plant tissues varied between 1.3 ± 0.8 and 94.0 ± 100.1 $\mu\text{g}\cdot\text{g}^{-1}$ dw and was very low in all plant leaves. *D. glomerata* roots held significantly higher NH_4^+ concentrations compared to *F. paniculata* (Figure 1b). Positive $\Delta^{17}\text{O}-\text{NO}_3^-$ in all tissues of both *D. glomerata* and *F. paniculata* evidences direct uptake of unprocessed $\text{NO}_3^-_{\text{atm}}$ (Figure 1c). The mean $\Delta^{17}\text{O}-\text{NO}_3^-$ ranged from 1.0 ± 0.7 ‰ in *D. glomerata* roots to 3.4 ± 3.2 ‰ in *F. paniculata* leaves. According to Eq. 1, the mean $\text{NO}_3^-_{\text{atm}}$ contribution accounted for 4 ± 3 % to 14 ± 13 %, and up to 33 % (when $\Delta^{17}\text{O} = 8.1$ ‰), of the NO_3^- pool in plant tissues (Figure 1c). *F. paniculata* exhibited similar high mean $\delta^{18}\text{O}-\text{NO}_3^-$ and $\delta^{15}\text{N}-\text{NO}_3^-$ in roots and leaves (Figure 1d and e). In *D. glomerata* leaves, the mean $\delta^{18}\text{O}-\text{NO}_3^-$ and $\delta^{15}\text{N}-\text{NO}_3^-$ spanned significantly higher values than in the roots.

The mean $[\text{NO}_3^-]$ in leaves was significantly higher after peak biomass in all plants (Figure 2a), whereas the mean $[\text{NH}_4^+]$ did not significantly vary (Figure 2b). The period after peak biomass was also characterized by significantly higher mean $\Delta^{17}\text{O}-\text{NO}_3^-$ in leaves and significantly lower mean $\delta^{15}\text{N}-\text{NO}_3^-$ in roots compared to the earlier period (Figures 2c and 2d). There was no significant difference for $\delta^{18}\text{O}-\text{NO}_3^-$ between the two periods (Figure S2).

Discussion

NO_3^- and $\text{NO}_3^-_{\text{atm}}$ uptake

One possible scenario that could explain the presence of $\text{NO}_3^-_{\text{atm}}$ in plant leaves involves direct foliar absorption of gaseous species (e.g., NO_2 , HNO_3) and/or the incorporation of $\text{NO}_3^-_{\text{atm}}$ dissolved in precipitation (Vallano & Sparks, 2007). The respective importance of each absorption pathways depends on a large array of leaf properties, among which the leaf wettability (i.e., the capacity to retain water). In both cases, these N compounds enter plant leaves following passive diffusion mechanisms either *via* the stomata or through the cuticle, depending on the chemical and physical

Accepted Article

characteristics of the pollutant and the leaf, and are eventually transformed into NO_3^- (Vallano & Sparks, 2007; Sparks, 2009). More important for this study, HNO_3 , NO_3^- , and, hypothetically, NO_2 lead to a similarly ^{17}O -enriched $\text{NO}_3^-_{\text{am}}$ when assimilated in leaves (Savarino *et al.*, 2008), regardless of the absorption pathway. Therefore, we will from now on use the term “foliar uptake of $\text{NO}_3^-_{\text{am}}$ ” to refer to the absorption of NO_3^- -producing species through the leaves, with no further consideration of the mechanism involved. This scenario is supported by a recent study of subalpine meadows in the French Pyrenees which highlighted the strong foliar uptake capacity of *Poaceae* (*i.e.*, *F. paniculata* and *D. glomerata* family) in an experiment where $\delta^{15}\text{N}$ -labeled NO_3^- and NH_4^+ were sprayed on natural subalpine grasslands (Pornon *et al.*, 2019).

Another possible scenario is the translocation of deposited $\text{NO}_3^-_{\text{am}}$ from soils to above-ground biomass (Pornon *et al.*, 2019). Root-to-shoot transport of NO_3^- *via* the xylem is well-documented for herbaceous species, with NO_3^- being either stored in petioles or reduced in mesophyll cells (Hachiya & Sakakibara, 2016). During translocation, NO_3^- can also be partly reduced in roots or stored in the vacuole. In our study, year-round positive $\Delta^{17}\text{O}-\text{NO}_3^-$ values in *D. glomerata* and *F. paniculata* roots suggest that at least part of the $\text{NO}_3^-_{\text{am}}$ in the plants was acquired *via* root uptake (Figure 1c).

However, $\Delta^{17}\text{O}-\text{NO}_3^-$ in leaves was significantly higher compared to roots after peak biomass (Figure 2c). Such a relationship can only be explained by foliar uptake being the dominant $\text{NO}_3^-_{\text{am}}$ assimilation pathway. Indeed, the enrichment of $\text{NO}_3^-_{\text{am}}$ in leaves (*i.e.*, increasing $\Delta^{17}\text{O}-\text{NO}_3^-$), if coming from a terrestrial reservoir, can only be caused by similar enrichment of $\text{NO}_3^-_{\text{am}}$ in this reservoir (*i.e.*, increasing $\Delta^{17}\text{O}-\text{NO}_3^-$), because biological and transport processes do not affect the $\Delta^{17}\text{O}$ value (Michalski *et al.*, 2004). We found that neither soils (Table 2) nor roots (Figure 2c) – which would be the reservoirs of $\text{NO}_3^-_{\text{am}}$ in leaves in this scenario – showed a similar increase in exogenous NO_3^- after peak biomass.

In order to further highlights the importance of foliar uptake of $\text{NO}_3^-_{\text{atm}}$ we introduce the terminology $X_{\text{leaves-roots}} = X_{\text{leaves}} - X_{\text{roots}}$, where X can be $[\text{NO}_3^-]$, $\Delta^{17}\text{O-NO}_3^-$, $\delta^{18}\text{O-NO}_3^-$ or $\delta^{15}\text{N-NO}_3^-$ at a given date. Here, $[\text{NO}_3^-]_{\text{leaves-roots}}$ and $\Delta^{17}\text{O-NO}_3^-_{\text{leaves-roots}}$ were positively correlated: $\Delta^{17}\text{O-NO}_3^-_{\text{leaves-roots}}$, and therefore f_{uptake} (Eq.4) increases with higher $[\text{NO}_3^-]_{\text{leaves-roots}}$ (Figure 3a). Foliar uptake of $\text{NO}_3^-_{\text{atm}}$ can therefore be quantified by considering the range of positive $\text{NO}_3^-_{\text{atm}}$ enrichment in leaves compared to roots, using Eq.4. When $\Delta^{17}\text{O}_{\text{leaves-roots}}$ is positive (*i.e.*, foliar uptake contributes more $\text{NO}_3^-_{\text{atm}}$ than root translocation), it spans a 0.9-3.8 ‰, corresponding to a $f_{\text{uptake}} = 4\text{-}16\%$.

Isotopic evidence of NO_3^- assimilation in roots and leaves

Uptake and subsequent transport of NO_3^- in plants is commonly regarded as yielding little, if any, isotopic fractionation due to the lack of bond breakage in these processes (Mariotti *et al.*, 1982; Evans *et al.*, 1996). Conversely, the co-variation of O and N isotopic fractionation can be a good indicator of biological processes such as denitrification (Wexler *et al.*, 2014; Fang *et al.*, 2015) and assimilation (Granger *et al.*, 2004, 2010). In plants, variations of $\delta^{18}\text{O-NO}_3^-$ and $\delta^{15}\text{N-NO}_3^-$ are mainly influenced by NO_3^- reduction (NR) into NH_4^+ in the protein-making process (Tcherkez & Farquhar, 2006). Laboratory and hydroponic experiments on NR-induced isotopic fractionation showed that $\delta^{18}\text{O-NO}_3^-$ and $\delta^{15}\text{N-NO}_3^-$ co-vary along a 1:1 slope (Karsh *et al.*, 2012; Estrada *et al.*, 2017). These findings were supported by the only field analysis of NR fractionation, where a slope of 1.27 was found between $\delta^{18}\text{O-NO}_3^-$ and $\delta^{15}\text{N-NO}_3^-$ in tree roots (Liu *et al.*, 2013b). Here, the linear regressions between $\delta^{18}\text{O-NO}_3^-_{\text{bio}}$ and $\delta^{15}\text{N-NO}_3^-_{\text{bio}}$ (see Eqs.5 and 6) showed similar slopes of 0.76 and 0.71 in species-aggregated roots and leaves, respectively (Figure 4a). These slopes were lower than the expected 1:1 line, suggesting the production and uptake of new $\text{NO}_3^-_{\text{bio}}$ with low $\delta^{18}\text{O}$ and $\delta^{15}\text{N}$. This was also found by Wexler *et al.* (2014) who reported weaker *in situ* denitrification slopes (0.4 - 0.7) compared to laboratory experiments (1.0) due to the production of new $\text{NO}_3^-_{\text{bio}}$ (see also Granger & Wankel, 2016). Here, the results suggest that constant uptake of new $\text{NO}_3^-_{\text{bio}}$ by roots and subsequent translocation to the leaves could account for the observed slopes.

In addition, the slope of 0.05 for the correlation between $\Delta^{17}\text{O-NO}_3^-$ and $\delta^{18}\text{O-NO}_3^-_{bio}$ further underscores the assimilation-driven $\delta^{18}\text{O}$ enrichment of $\text{NO}_3^-_{bio}$ in roots (Figure 4b). In the leaves, most $\delta^{18}\text{O-NO}_3^-$ values fall outside of the mixing line between $\text{NO}_3^-_{atm}$ and $\text{NO}_3^-_{bio}$ when most of the $\delta^{18}\text{O-NO}_3^-$ values in the roots fall on the mixing line (Figure 4b). This suggests that an additional assimilation step occurs in aboveground tissue after transport from the roots. This possible additional NR step in leaves is also supported by the significant correlation between $\delta^{18}\text{O}_{leaves-roots}$ and $\delta^{15}\text{N}_{leaves-roots}$ (0.99) and confirms $\text{NO}_3^-_{atm}$ metabolic reduction after foliar uptake (Figure 3b).

Different NO_3^- uptake patterns

Significantly higher $[\text{NH}_4^+]$ and lower $\delta^{15}\text{N-NO}_3^-$ in *D. glomerata* roots (Figure 1b and e) could reflect its exploitative strategy, characterized by fast uptake (*i.e.*, lower $\delta^{15}\text{N-NO}_3^-$ due to frequent turn-over with new $\text{NO}_3^-_{bio}$) and intensive NR rates (*i.e.*, production of in-tissue NH_4^+). The high $[\text{NH}_4^+]$ in *D. glomerata* roots could also stem from a particularly high NH_4^+ affinity (Grassein *et al.*, 2015), although no evidence exists that uptake and concentration of NH_4^+ are linked. TU meadows had the highest $[\text{NH}_4^+]$ in soils (Table 2) which may have favored NH_4^+ uptake by *D. glomerata* as N availability is a strong driver of N uptake strategy (Houlton *et al.*, 2007; Stahl *et al.*, 2011; Wang & Macko, 2011).

For *F. paniculata*, a more conservative species, the data showed a significantly higher f_{atm} in the roots (Figure 1c), mirroring the lower N cycling rates in UU soils previously documented (Robson *et al.*, 2007, 2010; Legay *et al.*, 2013), and the longer residence time of unprocessed $\text{NO}_3^-_{atm}$ illustrated by higher $\Delta^{17}\text{O-NO}_3^-$ in this meadow (Table 2). For this subalpine plant species growing in nutrient-poor soils (Table 2), uptake of $\text{NO}_3^-_{atm}$ appeared to be an important source of nutrients, a hypothesis also supported by higher f_{atm} in its leaves compared to *D. glomerata* (Figure 1c).

The higher f_{atm} in all plant leaves after peak biomass may indicate a shift in subalpine plants NO_3^- uptake pattern: root-based in spring after snowmelt, and leaf-based in summer when competition with microbial immobilization is stronger (Legay *et al.*, 2013) and the foliar surface for atmospheric exchange is at a maximum.

It remains unclear why $\delta^{15}\text{N}-\text{NO}_3^-$ in *D. glomerata* roots was lower than the estimated $\delta^{15}\text{N}-\text{NO}_3^-_{bio} = 5.1\text{‰}$ reported by Bourgeois *et al.*, (2018a) at the same site (Figure 4a and c). Because these low $\delta^{15}\text{N}-\text{NO}_3^-$ values span the reported $\delta^{15}\text{N}$ range of NO_3^- produced from $\text{NH}_4^+_{atm}$ nitrification (Figure 4a and c), it could indicate that $\text{NH}_4^+_{atm}$, along with NH_4^+ mineralized from organic N ($\text{NH}_4^+_{org}$), is an important substrate for nitrification (Bourgeois *et al.*, 2018a). Alternatively, low $\delta^{15}\text{N}-\text{NO}_3^-$ could be linked to the low nitrification rates in subalpine meadows (Robson *et al.*, 2007), leading to the production of $\delta^{15}\text{N}$ -depleted NO_3^- because of isotopic fractionation when the NH_4^+ pool is only partially nitrified (Mariotti *et al.*, 1981). Conversely, we found ^{15}N -enriched NO_3^- in *F. paniculata* roots compared to $\text{NO}_3^-_{bio}$ (Figure 4a), which could have resulted from several distinct or concomitant sources and processes:

(i) NO_3^- could be derived from manure as suggested by isotopic source partitioning (Figure 4a and c), but this is improbable considering the low occurrence of grazing and the absence of manuring in untended grasslands.

(ii) an association of *F. paniculata* with mycorrhizal fungi (Mouhamadou *et al.*, 2011; Binet *et al.*, 2013) may impact N and O isotopes of NO_3^- . However, the NR capacity of mycorrhizal fungi is expressed only in the presence of NO_3^- and absence of NH_4^+ (Liu *et al.*, 2014 and literature therein), which is not the case here. In addition, a review on the isotopic imprint of plant-fungal associations showed that mycorrhizal plants are ^{15}N -depleted (total N) compared to their fungal symbionts (Hobbie & Hogberg, 2012).

(iii) NO_3^- could stem from the storage of nutrients from previous years in tiller bases (Baptist *et al.*, 2013), ^{15}N -enriched by assimilation. This assumption is well supported by the slow N turnover in plant tissues in subalpine *Poaceae* (Pornon *et al.*, 2019), and by the year-round elevated $\delta^{15}\text{N}$ and $\delta^{18}\text{O}$ in *F. paniculata* (Figure 1d and e).

Whereas these results suggest a potentially significant correlation between root uptake of $\text{NO}_3^-_{\text{atm}}$ and $\text{NO}_3^-_{\text{bio}}$ and land use (probably due to different N speciation and availability; Table 2), the correlation between land-use trajectories and foliar uptake of $\text{NO}_3^-_{\text{atm}}$ was not evident in this study. The proportion of $\text{NO}_3^-_{\text{atm}}$ in leaves seemed to increase as the intensity of the land management decreased (along with N availability in soils, Table 2), although this result was not statistically significant (Figure 1c). A similar pattern was observed for $\delta^{18}\text{O}\text{-NO}_3^-$ (Figure 1d) and $\delta^{15}\text{N}\text{-NO}_3^-$ (Figure 1e). Additional work will be needed to further investigate this question.

Uncertainties and future work

In this work, isotopic mass balance calculations were limited to two grass species that were assumed to be most representative of plant communities in subalpine environments. Therefore, the variability in the significance of foliar absorption across the wide range of subalpine plant species was not specifically studied here. Since our study site is remote and far from N emissions, it would be interesting to study how foliar uptake varies with shifting abundances of atmospheric N_r species, for instance close to urban centers (with high NO_2) or agricultural zones (with high NH_3). Similar broad-scale studies like that by Liu *et al.* (2018) would be necessary to assess the variability of foliar $\text{NO}_3^-_{\text{atm}}$ uptake across ecosystems, and to elucidate the drivers of this variability (e.g., water content, N availability, N speciation in the atmosphere and in the soils). There is now compelling evidence that forest canopies exert a strong control on the proportion and speciation of atmospheric N reaching soils (Templer & Weathers, 2011; Rao *et al.*, 2014; Guerrieri *et al.*, 2015). Quantifying foliar uptake of atmospheric N from forest canopies would be a significant step toward understanding how elevated N

Accepted Article

deposition affects forested ecosystems. Another important aspect is the need to account for foliar NO_3^- uptake in N-limited environments subject to global changes. For instance, Mayor *et al.* (2017) demonstrated that global temperature increases may lead to a strong N/P decoupling in alpine soils above the tree line, which could be further exacerbated by foliar NO_3^- uptake, a variable not considered to date.

In the present study, we focused on the foliar uptake of NO_3^- . However, foliar uptake is also affected by other N species like PAN (Sparks *et al.*, 2003), other organic N compounds (Lockwood *et al.*, 2008) or NH_3 (Hanstein *et al.*, 1999; Pornon *et al.*, 2019). The 4-16 % range for foliar uptake of NO_3^- is but one part of the total foliar N uptake. Constraining the foliar uptake of these N species should be another important focus of future studies, especially given that their relative abundance in the atmosphere is changing (Li *et al.*, 2016).

Conclusion

The present study has advanced the current understanding of the potential NO_3^- absorption pathways by roots or leaves and their seasonal variability in subalpine plants, and has stressed the practical use of NO_3^- triple-isotope analyses to further our understanding of the role played by plants in the N biogeochemical cycle. We demonstrated that $\Delta^{17}\text{O}-\text{NO}_3^-$ in plant tissues is a powerful tool for constraining the direct foliar uptake of NO_3^- : two dominant subalpine plant species yielded an estimated foliar uptake of NO_3^- of 4-16 %. The simultaneous analysis of the triple isotopes of NO_3^- in plant tissues also provided a new perspective on plant functional biology, most notably on the NR process. We were able to show that NO_3^- assimilation occurs in both the roots and the leaves of subalpine plants. Our findings also suggest a seasonal variability in the respective contribution of N uptake pathways (roots vs. leaves), with greater assimilation occurring in the leaves after peak biomass, although further studies on this topic are needed. Results from this study bring new insights on the role of vegetation in the N balance in high-altitude catchments. We believe that the isotopic

This article is protected by copyright. All rights reserved.

approach used here could help improve the predictive capabilities of ecosystem models with regard to changing N deposition levels, if used on more plant species and at a larger scale.

Acknowledgments

This study was supported by grants from the Labex OSUG@2020 (“Investissements d’avenir” - ANR10 LABX56), the ARC – Environnement Région Rhone-Alpes and the Grenoble-Chambéry DIPEE CNRS. It was conducted at the Lautaret Garden (Station Alpine J. Fourier, Univ. Grenoble Alpes, CNRS, 38000 Grenoble, France), member of AnaEE-France (ANR-11-INBS-0001AnaEE-Services) and of the eLTER-Europe network (Univ. Grenoble Alpes, CNRS, LTSER Zone Atelier Alpes, 38000 Grenoble, France). We would like to thank N. Deschamps, C. Nesti, E. Vince and C. Arnoldi for helping with field and laboratory work and acknowledge J. Renaud for help with SIG and B. Mouhamadou for insightful discussion about plant-mycorrhizae associations. Finally, we acknowledge H. Angot and J. Peischl for their careful and precious English-editing of this manuscript.

Author contribution

IB, J-CC and JS designed the experiment. IB carried out the field work. IB and NC performed the laboratory analyses. IB analyzed the data. IB, JCC and JS discussed the results. IB wrote the paper, with revisions from JCC and JS.

References

- Aber JD, Nadelhoffer KJ, Steudler P, Melillo JM. 1989.** Nitrogen saturation in northern forest ecosystems. *BioScience* **39**: 378–386.
- Balestrini R, Arese C, Freppaz M, Buffagni A. 2013.** Catchment features controlling nitrogen dynamics in running waters above the tree line (central Italian Alps). *Hydrology and Earth System Sciences* **17**: 989–1001.
- Baptist F, Secher-Fromell H, Viard-Crétat F, Aranjuelo I, Clément J-C, Creme A, Desclos M, Laine P, Nogues S, Lavorel S. 2013.** Carbohydrate and nitrogen stores in *Festuca paniculata* under mowing explain dominance in subalpine grasslands. *Plant Biology* **15**: 395–404.
- Baron JS. 2006.** Hindcasting nitrogen deposition to determine an ecological critical load. *Ecological Applications* **16**: 433–439.
- Baron JS, Campbell DH. 1997.** Nitrogen fluxes in a high elevation Colorado Rocky Mountain basin. *Hydrological Processes* **11**: 783–799.
- Baron JS, Driscoll CT, Stoddard JL, Richer EE. 2011.** Empirical Critical Loads of Atmospheric Nitrogen Deposition for Nutrient Enrichment and Acidification of Sensitive US Lakes. *BioScience* **61**: 602–613.
- Bassin S, Volk M, Fuhrer J. 2013.** Species composition of subalpine grassland is sensitive to nitrogen deposition, but not to ozone, after seven years of treatment. *Ecosystems* **16**: 1105–1117.
- Binet MN, Sage L, Malan C, Clément JC, Redecker D, Wipf D, Geremia RA, Lavorel S, Mouhamadou B. 2013.** Effects of mowing on fungal endophytes and arbuscular mycorrhizal fungi in subalpine grasslands. *Fungal Ecology* **6**: 248–255.
- Bourgeois I, Savarino J, Caillon N, Angot H, Barbero A, Delbart F, Voisin D, Clément J-C. 2018a.** Tracing the fate of atmospheric nitrate in a subalpine watershed using $\Delta^{17}\text{O}$. *Environmental Science & Technology* **52**: 5561–5570.
- Bourgeois I, Savarino J, Némery J, Caillon N, Albertin S, Delbart F, Voisin D, Clément J-C. 2018b.** Atmospheric nitrate export in streams along a montane to urban gradient. *Science of The Total Environment* **633**: 329–340.
- Boutin M, Corcket E, Alard D, Villar L, Jiménez J-J, Blaix C, Lemaire C, Corriol G, Lamaze T, Pornon A. 2017.** Nitrogen deposition and climate change have increased vascular plant species richness and altered the composition of grazed subalpine grasslands. *Journal of Ecology* **105**: 1199–1209.
- Bowman WD, Gartner JR, Holland K, Wiedermann M. 2006.** Nitrogen critical loads for alpine vegetation and terrestrial ecosystem response: are we there yet? *Ecological Applications* **16**: 1183–1193.
- Burns DA. 2004.** The effects of atmospheric nitrogen deposition in the Rocky Mountains of Colorado and southern Wyoming, USA—a critical review. *Environmental Pollution* **127**: 257–269.
- Clark CM, Morefield PE, Gilliam FS, Pardo LH. 2013.** Estimated losses of plant biodiversity in the

United States from historical N deposition (1985–2010). *Ecology* **94**: 1441–1448.

Clément JC, Robson TM, Guillemin R, Saccone P, Lochet J, Aubert S, Lavorel S. 2012. The effects of snow-N deposition and snowmelt dynamics on soil-N cycling in marginal terraced grasslands in the French Alps. *Biogeochemistry* **108**: 297–315.

Clow DW, Roop HA, Nanus L, Fenn ME, Sexstone GA. 2015. Spatial patterns of atmospheric deposition of nitrogen and sulfur using ion-exchange resin collectors in Rocky Mountain National Park, USA. *Atmospheric Environment* **101**: 149–157.

Costa AW, Michalski G, Schauer AJ, Alexander B, Steig EJ, Shepson PB. 2011. Analysis of atmospheric inputs of nitrate to a temperate forest ecosystem from $\Delta^{17}\text{O}$ isotope ratio measurements. *Geophysical Research Letters* **38**: L15805.

Cui S, Shi Y, Groffman PM, Schlesinger WH, Zhu Y-G. 2013. Centennial-scale analysis of the creation and fate of reactive nitrogen in China (1910–2010). *Proceedings of the National Academy of Sciences* **110**: 2052–2057.

Dejwakh NR, Meixner T, Michalski G, McIntosh J. 2012. Using ^{17}O to investigate nitrate sources and sinks in a semi-arid groundwater system. *Environmental Science & Technology* **46**: 745–751.

Durka W, Schulze E-D, Gebauer G, Voerkeliust S. 1994. Effects of forest decline on uptake and leaching of deposited nitrate determined from ^{15}N and ^{18}O measurements. *Nature* **372**: 765–767.

Estrada NL, Böhlke JK, Sturchio NC, Gu B, Harvey G, Burkey KO, Grantz DA, McGrath MT, Anderson TA, Rao B, et al. 2017. Stable isotopic composition of perchlorate and nitrate accumulated in plants: hydroponic experiments and field data. *Science of The Total Environment* **595**: 556–566.

Evans RD, Bloom AJ, Sukrapanna SS, Ehleringer JR. 1996. Nitrogen isotope composition of tomato (*Lycopersicon esculentum* Mill. cv. T-5) grown under ammonium or nitrate nutrition. *Plant, Cell and Environment* **19**: 1317–1323.

Fang Y, Koba K, Makabe A, Takahashi C, Zhu W, Hayashi T, Hokari AA, Urakawa R, Bai E, Houlton BZ, et al. 2015. Microbial denitrification dominates nitrate losses from forest ecosystems. *Proceedings of the National Academy of Sciences* **112**: 1470–1474.

Fowler D, Coyle M, Skiba U, Sutton MA, Cape JN, Reis S, Sheppard LJ, Jenkins A, Grizzetti B, Galloway JN, et al. 2013. The global nitrogen cycle in the twenty-first century. *Philosophical Transactions of the Royal Society B: Biological Sciences* **368**: 20130164–20130164.

Fowler D, Steadman CE, Stevenson D, Coyle M, Rees RM, Skiba UM, Sutton MA, Cape JN, Dore AJ, Vieno M, et al. 2015. Effects of global change during the 21st century on the nitrogen cycle. *Atmospheric Chemistry and Physics* **15**: 13849–13893.

Galloway JN, Aber JD, Erisman JW, Seitzinger SP, Howarth RW, Cowling EB, Cosby BJ. 2003. The Nitrogen Cascade. *BioScience* **53**: 341.

Galloway JN, Dentener FJ, Capone DG, Boyer EW, Howarth RW, Seitzinger SP, Asner GP, Cleveland CC, Green PA, Holland EA, et al. 2004. Nitrogen cycles: past, present, and future. *Biogeochemistry*

70: 153–226.

Galloway JN, Townsend AR, Erisman JW, Bekunda M, Cai Z, Freney JR, Martinelli LA, Seitzinger SP, Sutton MA. 2008. Transformation of the nitrogen cycle: recent trends, questions, and potential solutions. *Science* **320**: 889–892.

Granger J, Sigman DM, Needoba JA, Harrison PJ. 2004. Coupled nitrogen and oxygen isotope fractionation of nitrate during assimilation by cultures of marine phytoplankton. *Limnology and Oceanography* **49**: 1763–1773.

Granger J, Sigman DM, Rohde MM, Maldonado MT, Tortell PD. 2010. N and O isotope effects during nitrate assimilation by unicellular prokaryotic and eukaryotic plankton cultures. *Geochimica et Cosmochimica Acta* **74**: 1030–1040.

Granger J, Wankel SD. 2016. Isotopic overprinting of nitrification on denitrification as a ubiquitous and unifying feature of environmental nitrogen cycling. *Proceedings of the National Academy of Sciences* **113**: E6391–E6400.

Grassein F, Lemauviel-Lavenant S, Lavorel S, Bahn M, Bardgett RD, Desclos-Theveniau M, Laine P. 2015. Relationships between functional traits and inorganic nitrogen acquisition among eight contrasting European grass species. *Annals of Botany* **115**: 107–115.

Guerrieri R, Vanguelova EI, Michalski G, Heaton THE, Mencuccini M. 2015. Isotopic evidence for the occurrence of biological nitrification and nitrogen deposition processing in forest canopies. *Global Change Biology* **21**: 4613–4626.

Hachiya T, Sakakibara H. 2016. Interactions between nitrate and ammonium in their uptake, allocation, assimilation, and signaling in plants. *Journal of Experimental Botany* **68**: 2501–2512.

Hanstein S, Mattsson M, Jaeger H-J, Schjoerring JK. 1999. Uptake and utilization of atmospheric ammonia in three native Poaceae species: leaf conductances, composition of apoplastic solution and interactions with root nitrogen supply. *New Phytologist* **141**: 71–83.

Hastings MG, Jarvis JC, Steig EJ. 2009. Anthropogenic impacts on nitrogen isotopes of ice-core nitrate. *Science* **324**: 1288–1288.

Hobbie EA, Hogberg P. 2012. Nitrogen isotopes link mycorrhizal fungi and plants to nitrogen dynamics. *New Phytologist* **196**: 367–382.

Holland E, Guenther B, Lee-Taylor M, Bertman S, Carroll M, Shepson P, Sparks J. 2005. U.S. nitrogen science plan focuses collaborative efforts. *Eos* **86**: 253–260.

Hood EW, Williams MW, Caine N. 2003. Landscape Controls on Organic and Inorganic Nitrogen Leaching across an Alpine/Subalpine Ecotone, Green Lakes Valley, Colorado Front Range. *Ecosystems* **6**: 0031–0045.

Houlton BZ, Sigman DM, Schuur EAG, Hedin LO. 2007. A climate-driven switch in plant nitrogen acquisition within tropical forest communities. *Proceedings of the National Academy of Sciences* **104**: 8902–8906.

This article is protected by copyright. All rights reserved.

Kaiser J, Hastings MG, Houlton BZ, Röckmann T, Sigman DM. 2007. Triple oxygen isotope analysis of nitrate using the denitrifier method and thermal decomposition of N₂O. *Analytical Chemistry* **79**: 599–607.

Karsh KL, Granger J, Kritee K, Sigman DM. 2012. Eukaryotic assimilatory nitrate reductase fractionates N and O isotopes with a ratio near unity. *Environmental Science & Technology* **46**: 5727–5735.

Kaye JP, Hart SC. 1997. Competition for nitrogen between plants and soil microorganisms. *Trends in Ecology & Evolution* **12**: 139–143.

Kendall C, Elliott EM, Wankel SD. 2007. Tracing anthropogenic inputs of nitrogen to ecosystems. *Stable isotopes in ecology and environmental science* **2**: 375–449.

Legay N, Grassein F, Robson TM, Personeni E, Bataillé M-P, Lavorel S, Clément J-C. 2013. Comparison of inorganic nitrogen uptake dynamics following snowmelt and at peak biomass in subalpine grasslands. *Biogeosciences* **10**: 7631–7645.

Legay N, Lavorel S, Baxendale C, Krainer U, Bahn M, Binet M-N, Cantarel AAM, Colace M-P, Foulquier A, Kastl E-M, et al. 2016. Influence of plant traits, soil microbial properties, and abiotic parameters on nitrogen turnover of grassland ecosystems. *Ecosphere* **7**: e01448.

Li Y, Schichtel BA, Walker JT, Schwede DB, Chen X, Lehmann CMB, Puchalski MA, Gay DA, Collett JL. 2016. Increasing importance of deposition of reduced nitrogen in the United States. *Proceedings of the National Academy of Sciences* **113**: 5874–5879.

Liu X-Y, Koba K, Koyama LA, Hobbie SE, Weiss MS, Inagaki Y, Shaver GR, Giblin AE, Hobara S, Nadelhoffer KJ, et al. 2018. Nitrate is an important nitrogen source for Arctic tundra plants. *Proceedings of the National Academy of Sciences of the United States of America* **115**: 3398–3403.

Liu X-Y, Koba K, Liu C-Q, Li X-D, Yoh M. 2012a. Pitfalls and new mechanisms in moss isotope biomonitors of atmospheric nitrogen deposition. *Environmental Science & Technology* **46**: 12557–12566.

Liu X-Y, Koba K, Makabe A, Li X-D, Yoh M, Liu C-Q. 2013a. Ammonium first: natural mosses prefer atmospheric ammonium but vary utilization of dissolved organic nitrogen depending on habitat and nitrogen deposition. *New Phytologist* **199**: 407–419.

Liu X-Y, Koba K, Makabe A, Liu C-Q. 2014. Nitrate dynamics in natural plants: insights based on the concentration and natural isotope abundances of tissue nitrate. *Frontiers in Plant Science* **5**: 355.

Liu X-Y, Koba K, Takebayashi Y, Liu C-Q, Fang Y-T, Yoh M. 2012b. Preliminary insights into $\delta^{15}\text{N}$ and $\delta^{18}\text{O}$ of nitrate in natural mosses: a new application of the denitrifier method. *Environmental Pollution* **162**: 48–55.

Liu X-Y, Koba K, Takebayashi Y, Liu C-Q, Fang Y-T, Yoh M. 2013b. Dual N and O isotopes of nitrate in natural plants: first insights into individual variability and organ-specific patterns. *Biogeochemistry* **114**: 399–411.

- Liu X-Y, Koba K, Yoh M, Liu C-Q. 2013c.** Nitrogen and oxygen isotope effects of tissue nitrate associated with nitrate acquisition and utilisation in the moss *Hypnum plumaeforme*. *Functional Plant Biology* **39**: 598.
- Lockwood AL, Filley TR, Rhodes D, Shepson PB. 2008.** Foliar uptake of atmospheric organic nitrates. *Geophysical Research Letters* **35**: L15809.
- Mariotti A, Germon JC, Hubert P, Kaiser P, Letolle R, Tardieux A, Tardieux P. 1981.** Experimental determination of nitrogen kinetic isotope fractionation: some principles; illustration for the denitrification and nitrification processes. *Plant and soil* **62**: 413–430.
- Mariotti A, Mariotti F, Champigny M-L, Amarger N, Moysé A. 1982.** Nitrogen isotope fractionation associated with nitrate reductase activity and uptake of NO₃⁻ by Pearl Millet. *Plant Physiology* **69**: 880–884.
- Mast MA, Clow DW, Baron JS, Wetherbee GA. 2014.** Links between N deposition and nitrate export from a high-elevation watershed in the Colorado Front Range. *Environmental Science & Technology* **48**: 14258–14265.
- Mayer B, Boyer EW, Goodale C, Jaworski NA, Van Breemen N, Howarth RW, Seitzinger S, Billen G, Lajtha K, Nadelhoffer K, et al. 2002.** Sources of nitrate in rivers draining sixteen watersheds in the northeastern US: isotopic constraints. *Biogeochemistry* **57**: 171–197.
- Mayor JR, Sanders NJ, Classen AT, Bardgett RD, Clément J-C, Fajardo A, Lavorel S, Sundqvist MK, Bahn M, Chisholm C, et al. 2017.** Elevation alters ecosystem properties across temperate treelines globally. *Nature* **542**: 91–95.
- Michalski G, Meixner T, Fenn M, Hernandez L, Sirulnik A, Allen E, Thiemens M. 2004.** Tracing atmospheric nitrate deposition in a complex semiarid ecosystem using $\Delta^{17}\text{O}$. *Environmental Science & Technology* **38**: 2175–2181.
- Miller MF. 2002.** Isotopic fractionation and the quantification of ¹⁷O anomalies in the oxygen three-isotope system: an appraisal and geochemical significance. *Geochimica et Cosmochimica Acta* **66**: 1881–1889.
- Mladenov N, Williams MW, Schmidt SK, Cawley K. 2012.** Atmospheric deposition as a source of carbon and nutrients to an alpine catchment of the Colorado Rocky Mountains. *Biogeosciences* **9**: 3337–3355.
- Morin S, Savarino J, Frey MM, Yan N, Bekki S, Bottenheim JW, Martins JMF. 2008.** Tracing the origin and fate of NO_x in the Arctic atmosphere using stable isotopes in nitrate. *Science* **322**: 730–732.
- Mouhamadou B, Molitor C, Baptist F, Sage L, Clément J-C, Lavorel S, Monier A, Geremia RA. 2011.** Differences in fungal communities associated to *Festuca paniculata* roots in subalpine grasslands. *Fungal Diversity* **47**: 55–63.
- Nanus L, Campbell DH, Lehmann CMB, Mast MA. 2018.** Spatial and temporal variation in sources of atmospheric nitrogen deposition in the Rocky Mountains using nitrogen isotopes. *Atmospheric*

Environment **176**: 110–119.

Nanus L, McMurray JA, Clow DW, Saros JE, Blett T, Gurdak JJ. 2017. Spatial variation of atmospheric nitrogen deposition and critical loads for aquatic ecosystems in the Greater Yellowstone Area. *Environmental Pollution* **223**: 644–656.

Nanus L, Williams MW, Campbell DH, Elliott EM, Kendall C. 2008. Evaluating regional patterns in nitrate sources to watersheds in national parks of the Rocky Mountains using nitrate isotopes. *Environmental Science & Technology* **42**: 6487–6493.

Pornon A, Boutin M, Lamaze T. 2019. Contribution of plant species to the high N retention capacity of a subalpine meadow undergoing elevated N deposition and warming. *Environmental Pollution* **245**: 235–242.

Quétier F, Thébault A, Lavorel S. 2007. Plant traits in a state and transition framework as markers of ecosystem response to land-use change. *Ecological Monographs* **77**: 33–52.

Rao P, Hutyra LR, Raciti SM, Templer PH. 2014. Atmospheric nitrogen inputs and losses along an urbanization gradient from Boston to Harvard Forest, MA. *Biogeochemistry* **121**: 229–245.

Riha KM, Michalski G, Gallo EL, Lohse KA, Brooks PD, Meixner T. 2014. High atmospheric nitrate inputs and nitrogen turnover in semi-arid urban catchments. *Ecosystems* **17**: 1309–1325.

Robson TM, Baptist F, Clément J-C, Lavorel S. 2010. Land use in subalpine grasslands affects nitrogen cycling via changes in plant community and soil microbial uptake dynamics. *Journal of Ecology* **98**: 62–73.

Robson T, Lavorel S, Clément J-C, Roux X. 2007. Neglect of mowing and manuring leads to slower nitrogen cycling in subalpine grasslands. *Soil Biology and Biochemistry* **39**: 930–941.

Rose LA, Sebestyen SD, Elliott EM, Koba K. 2015. Drivers of atmospheric nitrate processing and export in forested catchments. *Water Resources Research* **51**: 1333–1352.

Savarino J, Bhattacharya SK, Morin S, Baroni M, Doussin J-F. 2008. The NO+O₃ reaction: a triple oxygen isotope perspective on the reaction dynamics and atmospheric implications for the transfer of the ozone isotope anomaly. *The Journal of Chemical Physics* **128**: 194303.

Savarino J, Morin S, Erbland J, Grannec F, Patey MD, Vicars W, Alexander B, Achterberg EP. 2013. Isotopic composition of atmospheric nitrate in a tropical marine boundary layer. *Proceedings of the National Academy of Sciences* **110**: 17668–17673.

Sparks JP. 2009. Ecological ramifications of the direct foliar uptake of nitrogen. *Oecologia* **159**: 1–13.

Sparks JP, Roberts JM, Monson RK. 2003. The uptake of gaseous organic nitrogen by leaves: A significant global nitrogen transfer process. *Geophysical Research Letters* **30**: 23, 2189.

Stahl VM, Beyschlag W, Werner C. 2011. Dynamic niche sharing in dry acidic grasslands - a ¹⁵N-labeling experiment. *Plant and Soil* **1–2**: 389–400.

Tcherkez G, Farquhar GD. 2006. *Viewpoint* : Isotopic fractionation by plant nitrate reductase, twenty

years later. *Functional Plant Biology* **33**: 531.

Templer PH, Weathers KC. 2011. Use of mixed ion exchange resin and the denitrifier method to determine isotopic values of nitrate in atmospheric deposition and canopy throughfall. *Atmospheric Environment* **45**: 2017–2020.

Thébault A, Clément J-C, Ibanez S, Roy J, Geremia RA, Pérez CA, Buttler A, Estienne Y, Lavorel S. 2014. Nitrogen limitation and microbial diversity at the treeline. *Oikos* **123**: 729–740.

Tsunogai U, Komatsu DD, Daita S, Kazemi GA, Nakagawa F, Noguchi I, Zhang J. 2010. Tracing the fate of atmospheric nitrate deposited onto a forest ecosystem in Eastern Asia using $\Delta^{17}\text{O}$. *Atmospheric Chemistry and Physics* **10**: 1809–1820.

Tsunogai U, Miyauchi T, Ohyama T, Komatsu DD, Nakagawa F, Obata Y, Sato K, Ohizumi T. 2016. Accurate and precise quantification of atmospheric nitrate in streams draining land of various uses by using triple oxygen isotopes as tracers. *Biogeosciences* **13**: 3441–3459.

Vallano DM, Sparks JP. 2007. Foliar $\delta^{15}\text{N}$ values as indicators of foliar uptake of atmospheric nitrogen pollution. *Terrestrial Ecology* **1**: 93–109.

Vicars WC, Savarino J. 2014. Quantitative constraints on the ^{17}O -excess ($\Delta^{17}\text{O}$) signature of surface ozone: ambient measurements from 50°N to 50°S using the nitrite-coated filter technique. *Geochimica et Cosmochimica Acta* **135**: 270–287.

Vitousek PM, Aber JD, Howarth RW, Likens GE, Matson PA, Schindler DW, Schlesinger WH, Tilman DG. 1997. Human alteration of the global nitrogen cycle: sources and consequences. *Ecological Applications* **7**: 737–750.

Wang L, Macko SA. 2011. Constrained preferences in nitrogen uptake across plant species and environments. *Plant, Cell & Environment* **34**: 525–534.

Wankel SD, Kendall C, Francis CA, Paytan A. 2006. Nitrogen sources and cycling in the San Francisco Bay Estuary: a nitrate dual isotopic composition approach. *Limnology and Oceanography* **51**: 1654–1664.

Ward MH, deKok TM, Levallois P, Brender J, Gulis G, Nolan BT, VanDerslice J. 2005. Workgroup Report: drinking-water nitrate and health—recent findings and research needs. *Environmental Health Perspectives* **113**: 1607–1614.

Weintraub SR, Brooks PD, Bowen GJ. 2017. Interactive effects of vegetation type and topographic position on nitrogen availability and loss in a temperate montane ecosystem. *Ecosystems* **20**: 1073–1088.

Wexler SK, Goodale CL, McGuire KJ, Bailey SW, Groffman PM. 2014. Isotopic signals of summer denitrification in a northern hardwood forested catchment. *Proceedings of the National Academy of Sciences* **111**: 16413–16418.

Williams MW, Tonnessen KA. 2000. Critical loads for inorganic nitrogen deposition in the Colorado Front Range, USA. *Ecological Applications* **10**: 1648–1665.

This article is protected by copyright. All rights reserved.

Supplementary Figures

Figure S1 Map of the Lautaret pass study area.

Figure S2 Before and after peak biomass values of $\delta^{18}\text{O}\text{-NO}_3^-$ (‰) in pooled *F. paniculata* and *D. glomerata* plant leaves and roots.

List of Figures

Figure 1 Annual statistics of (a) $[\text{NO}_3^-]$ ($\mu\text{g}\cdot\text{g}^{-1}$ dw), (b) $[\text{NH}_4^+]$ ($\mu\text{g}\cdot\text{g}^{-1}$ dw), (c) $\Delta^{17}\text{O}$ (‰) and corresponding f_{am} (%), the proportion of $\text{NO}_3^-_{\text{am}}$, (d) $\delta^{18}\text{O}$ (‰) and (e) $\delta^{15}\text{N}$ (‰) of NO_3^- in *D. glomerata* and *F. paniculata* leaves (n = 55 and 33 for concentration and isotopic data, respectively) and roots (n = 56 and 47 for concentration and isotopic data, respectively), sampled between May and September 2016. Box plots show the weighted mean, as well as the 25th and 75th percentiles. Different letters indicate significant differences between plant species for the same biological tissue (leaves or roots). Asterisks indicate significant differences between plant tissues for a given species: *, p<0.05; **, p<0.01; ***, p<0.001).

Figure 2 Pre- and post-peak biomass statistics of (a) $[\text{NO}_3^-]$ ($\mu\text{g}\cdot\text{g}^{-1}$ dry tissue), (b) $[\text{NH}_4^+]$ ($\mu\text{g}\cdot\text{g}^{-1}$ dry tissue), (c) $\Delta^{17}\text{O}\text{-NO}_3^-$ (‰) and corresponding f_{am} (%), the proportion of $\text{NO}_3^-_{\text{am}}$ and (d) $\delta^{15}\text{N}\text{-NO}_3^-$ (‰) in pooled *Festuca paniculata* and *Dactylis glomerata* leaves (green) and roots (brown). Box plots show the mean, as well as the 25th and 75th percentiles. The black arrow indicates the occurrence of peak biomass (early July). The grey area marks the post-peak biomass period. Different letters indicate significant differences (p<0.05) in values for the same biological tissue (leaves or roots) between the two periods. Asterisks indicate significant differences between plant tissues (roots vs. leaves) for a given period: *, p<0.05; **, p<0.01; ***, p<0.001.

Figure 3 Differences between leaves and roots of (a) $\Delta^{17}\text{O}\text{-NO}_3^-$ (‰) vs. $[\text{NO}_3^-]$ ($\mu\text{g}\cdot\text{g}^{-1}$ dw) and (b) $\delta^{18}\text{O}\text{-NO}_3^-$ (‰) vs. $\delta^{15}\text{N}\text{-NO}_3^-$ (‰). Samples are either DG-TM (*Dactylis glomerata* from Terraced-Mown meadows), DG-TU (*D. glomerata* from Terraced-Unmown meadows), and FP-UU (*Festuca paniculata* from Unterraced-Unmown meadows). In (a) the regression line illustrates the correlation between NO_3^- enrichment in leaves compared to roots and $\Delta^{17}\text{O}\text{-NO}_3^-$ enrichment in leaves compared

to roots (indicating foliar uptake of $\text{NO}_3^-_{am}$). In (b) $\text{NO}_3^-_{bio}$ isotopic values that have been corrected for $\text{NO}_3^-_{am}$ contribution (see Methods section for details) are shown in red (in black are the uncorrected values). The linear regression slope of 0.99 highlights the additional assimilation step occurring in leaves. Note that each data point corresponds the mean value of three plant individuals per sampling date.

Figure 4 Root (brown) and leaf (green) NO_3^- isotopic values showing (a) $\delta^{18}\text{O}$ (‰) vs. $\delta^{15}\text{N}$ (‰), (b) $\Delta^{17}\text{O}$ (‰) vs. $\delta^{18}\text{O}$ (‰) and (c) $\Delta^{17}\text{O}$ (‰) vs. $\delta^{15}\text{N}$ (‰). The three different plant species are represented by three different symbols (see legend). The plant species/land-use trajectory combinations are represented by three different symbols (see legend). TM refers to Terraced-Mown land-use, TU to Terraced-Unmown land-use, and UU to Unterraced-Unmown land-use. In (a) the isotopic ranges of NO_3^- produced from different ammonium sources are indicated by rectangles (cf., (Kendall *et al.*, 2007)). The colors correspond to: grey = NO_3^- from atmospheric ammonium ($\text{NH}_4^+_{am}$), turquoise = NO_3^- from mineralized organic matter ($\text{NH}_4^+_{org}$), beige = NO_3^- from manure NH_4^+ . In (b) and (c), the same grey, turquoise and beige colors are used to delineate the areas of mixing between the atmospheric end-member (*i.e.*, 100% $\text{NO}_3^-_{am}$), represented by the blue diamond, and the other NO_3^- sources mentioned above (*i.e.*, 100% $\text{NO}_3^-_{bio}$). Note the overlapping mixing ranges in (b). The atmospheric end-member (blue diamond) represents to the mean isotopic values of deposited $\text{NO}_3^-_{am}$ at the Lautaret pass (Table 1). In all panels, the red diamond corresponds to the isotopic values of $\text{NO}_3^-_{bio}$ at the Lautaret pass as measured by Bourgeois *et al.* (2018). The dashed arrows indicate the expected isotopic effect of NO_3^- assimilation on $\delta^{18}\text{O}$ - NO_3^- (enrichment), $\delta^{15}\text{N}$ - NO_3^- (enrichment), and $\Delta^{17}\text{O}$ - NO_3^- (no effect). Measurements located within a mixing range correspond to plant NO_3^- samples containing a mixture of $\text{NO}_3^-_{am}$ and $\text{NO}_3^-_{bio}$. Data points located outside a mixing range correspond to plant NO_3^- samples that were isotopically fractionated (*e.g.*, through assimilation). When significant, the regression lines between sample isotopic values were plotted for leaves (green) and roots (brown). Note that each data point represents the mean value of three plant individuals per sampling date.

Table 1 Mean NO_3^- and NH_4^+ concentrations and NO_3^- isotopic values, and associated standard deviation, in wet and dry deposition collected at the Lautaret Pass from May to September 2016.

Deposition	$[\text{NO}_3^-]$ ($\text{mg}\cdot\text{L}^{-1}$)	$[\text{NH}_4^+]$ ($\text{mg}\cdot\text{L}^{-1}$)	$\Delta^{17}\text{O}$ (‰)	$\delta^{18}\text{O}$ (‰)	$\delta^{15}\text{N}$ (‰)
Dry deposition (n=10)	-	-	25.1 ± 2.7	69.1 ± 5.7	-5.1 ± 6.2
Wet deposition (n=9)	5.5 ± 3.2	0.5 ± 0.2	23.6 ± 2.0	63.8 ± 6.0	-7.1 ± 1.7
Atmospheric end-member	-	-	24.4 ± 2.4	66.6 ± 5.8	-6.0 ± 4.1

Under is shown the inferred isotopic values for this study atmospheric end-member.

Table 2 Weighted mean annual concentration of NO_3^- and NH_4^+ ($\mu\text{g}\cdot\text{g}^{-1}$ dw) and concentration-weighted isotopic values of NO_3^- (‰) in soil extracts and associated standard deviation.

Soils extracts	$[\text{NO}_3^-]$ ($\mu\text{g}\cdot\text{g}^{-1}$ dw)	$[\text{NH}_4^+]$ ($\mu\text{g}\cdot\text{g}^{-1}$ dw)	$\Delta^{17}\text{O}$ (‰)	$\delta^{18}\text{O}$ (‰)	$\delta^{15}\text{N}$ (‰)
UU meadows (n=18)	14.6 ± 19.0	13.0 ± 13.7	0.9 ± 0.6	-4.3 ± 6.8	-5.1 ± 6.6
TU meadows (n=21)	58.9 ± 46.9	17.5 ± 29.9	0.5 ± 0.8	-10.3 ± 6.6	-1.3 ± 9.6
TM meadows (n=21)	52.3 ± 48.7	6.2 ± 4.0	0.3 ± 0.4	-10.9 ± 5.1	-2.6 ± 6.5

UU, Unterraced-Unmown; TU, Terraced-Unmown; TM, Terraced-Mown land-use trajectories.

List of Figures

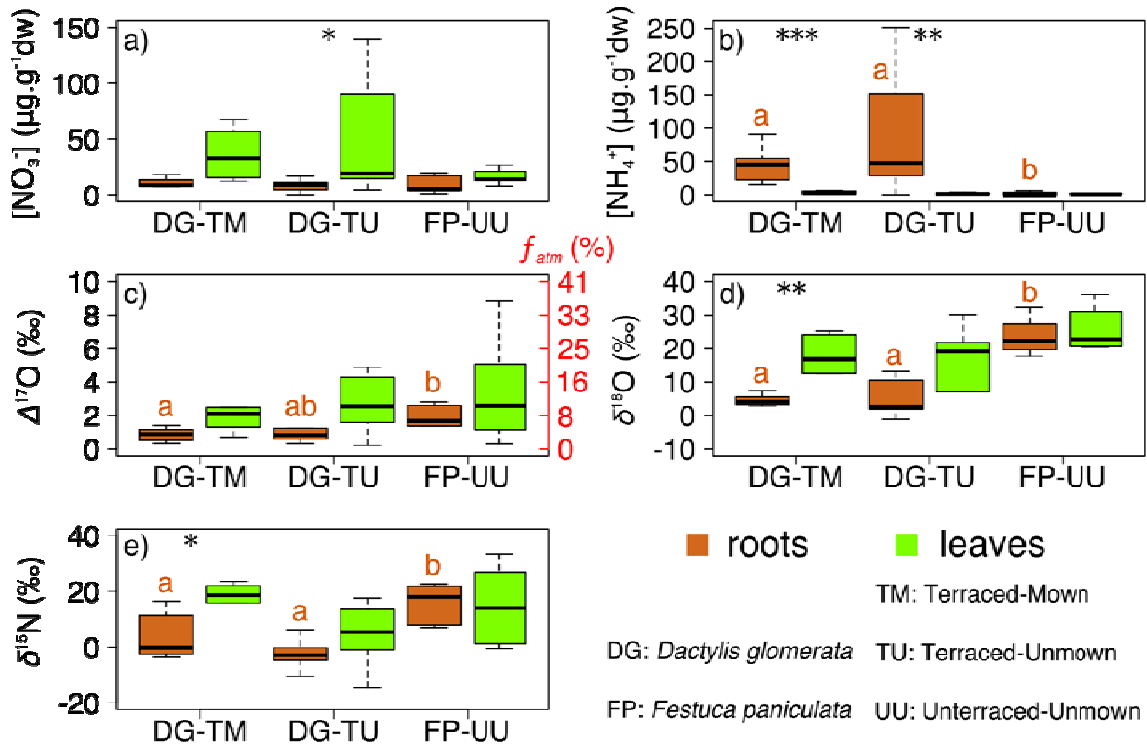


Figure 1 Annual mean a) $[NO_3^-]$ ($\mu\text{g}\cdot\text{g}^{-1}\text{dw}$), b) $[NH_4^+]$ ($\mu\text{g}\cdot\text{g}^{-1}\text{dw}$), c) $\Delta^{17}O$ (‰) and corresponding f_{atm} (%), the proportion of $NO_3^-_{atm}$, d) $\delta^{18}O$ (‰) and e) $\delta^{15}N$ (‰) of NO_3^- in *D. glomerata* and *F. paniculata* leaves (n = 55 and 33 for concentration and isotopic data, respectively) and roots (n = 56 and 47 for concentration and isotopic data, respectively), sampled between May and September 2016. Box plots show the mean, as well as the 25th and 75th percentiles. Different letters indicate significant differences between plant species for the same biological tissue (leaves or roots). Asterisks indicate significant differences between plant tissues for a given species (* for $p < 0.05$, ** for $p < 0.01$, *** for $p < 0.001$).

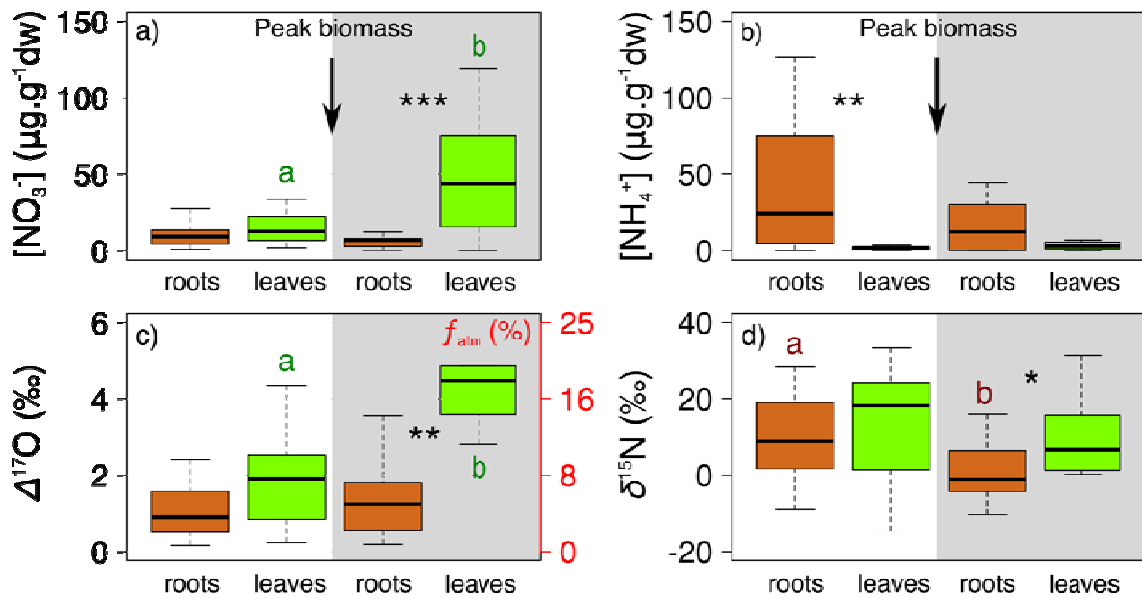


Figure 2 Pre- and post-peak biomass values of a) $[\text{NO}_3^-]$ ($\mu\text{g.g}^{-1}$ dry tissue), b) $[\text{NH}_4^+]$ ($\mu\text{g.g}^{-1}$ dry tissue), c) $\Delta^{17}\text{O-NO}_3^-$ (‰) and corresponding f_{ami} (%), the proportion of $\text{NO}_3^-_{ami}$ and d) $\delta^{15}\text{N-NO}_3^-$ (‰) in pooled *F. paniculata* and *D. glomerata* leaves (green) and roots (brown). Box plots show the mean, as well as the 25th and 75th percentiles. The black arrow indicates the occurrence of peak biomass (early July). The grey area marks the post-peak biomass period. Different letters indicate significant differences ($p < 0.05$) in values for the same biological tissue (leaves or roots) between the two periods. Asterisks indicate significant differences between plant tissues (roots vs. leaves) for a given period (* for $p < 0.05$, ** for $p < 0.01$, *** for $p < 0.001$).

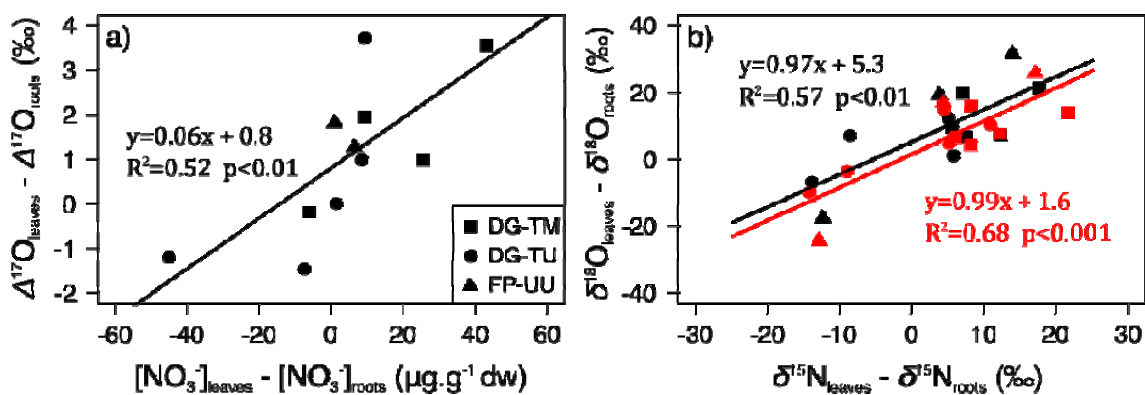


Figure 3 Differences between leaves and roots of a) $\Delta^{17}\text{O}-\text{NO}_3^-$ (‰) vs. $[\text{NO}_3^-]$ ($\mu\text{g}\cdot\text{g}^{-1}$ dw) and b) $\delta^{18}\text{O}-\text{NO}_3^-$ (‰) vs. $\delta^{15}\text{N}-\text{NO}_3^-$ (‰). Samples are either DG-TM (*D. glomerata* from Terraced-Mown meadows), DG-TU (*D. glomerata* from Terraced-Unmown meadows), and FP-UU (*F. paniculata* from Unterraced-Unmown meadows).

In a) the regression line illustrates the correlation between NO_3^- enrichment in leaves compared to roots and $\Delta^{17}\text{O}-\text{NO}_3^-$ enrichment in leaves compared to roots (indicating foliar uptake of $\text{NO}_3^-_{\text{atm}}$). In b) $\text{NO}_3^-_{\text{bio}}$ isotopic values that have been corrected for $\text{NO}_3^-_{\text{atm}}$ contribution (see Methods section for details) are shown in red (in black are the uncorrected values). The linear regression slope of 0.99 highlights the additional assimilation step occurring in leaves. Note that each data point corresponds to the mean value of three plant individuals per sampling date.

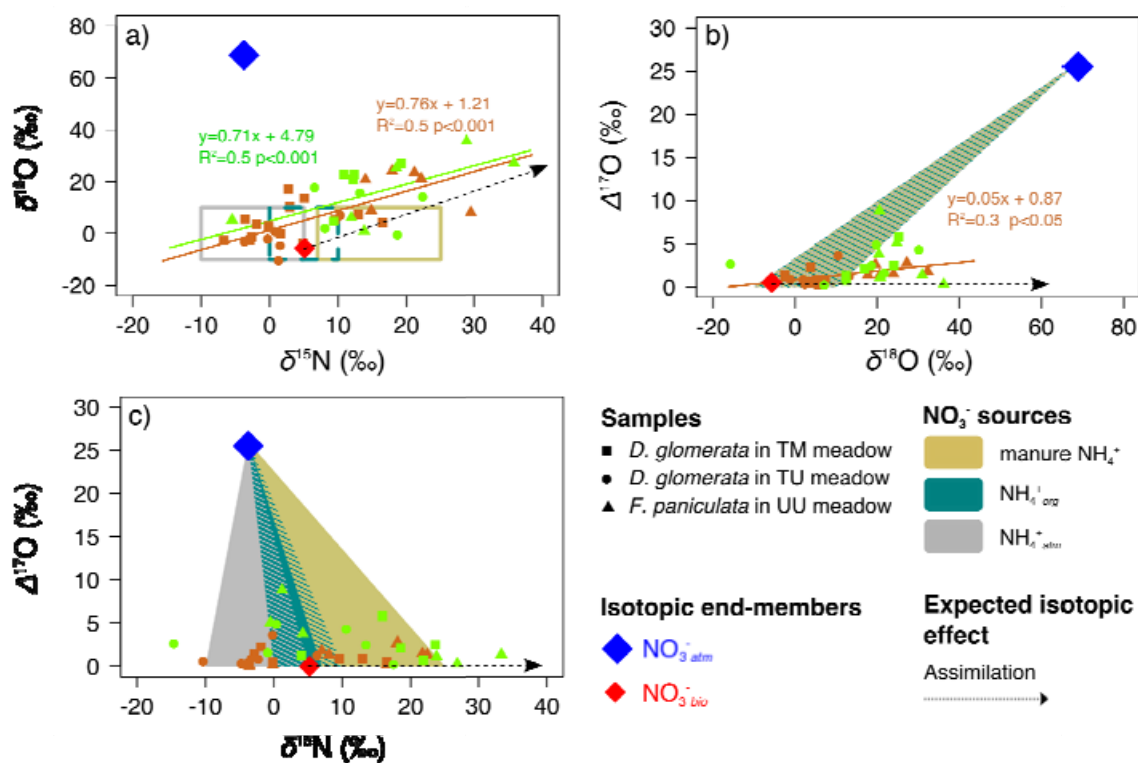


Figure 4 Root (brown) and leaf (green) NO_3^- isotopic values showing a) $\delta^{18}\text{O}$ (‰) vs. $\delta^{15}\text{N}$ (‰), b) $\Delta^{17}\text{O}$ (‰) vs. $\delta^{18}\text{O}$ (‰) and c) $\Delta^{17}\text{O}$ (‰) vs. $\delta^{15}\text{N}$ (‰). The plant species/land-use trajectory combinations are represented by three different symbols (see legend). TM refers to Terraced-Mown land-use, TU to Terraced-Unmown land-use, and UU to Unterraced-Unmown land-use.

In a) the isotopic ranges of NO_3^- produced from different ammonium sources are indicated by rectangles (cf., (Kendall *et al.*, 2007)). The colors correspond to: grey = NO_3^- from atmospheric ammonium (NH_4^+ atm), turquoise = NO_3^- from mineralized organic matter (NH_4^+ org), beige = NO_3^- from manure NH_4^+ . In b) and c), the same grey, turquoise and beige colors are used to delineate the areas of mixing between the atmospheric end-member (i.e., 100% NO_3^- atm), represented by the blue diamond, and the other NO_3^- sources mentioned above (i.e., 100% NO_3^- bio). Note the overlapping mixing ranges in b). The atmospheric end-member (blue diamond) represents to the mean isotopic values of deposited NO_3^- atm at the Lautaret pass (Table S1). In all panels, the red diamond corresponds to the isotopic values of NO_3^- bio at the Lautaret pass as measured by Bourgeois *et al.* (2018). The dashed arrows indicate the expected isotopic effect of NO_3^- assimilation on $\delta^{18}\text{O}$ - NO_3^- (enrichment), $\delta^{15}\text{N}$ - NO_3^- (enrichment), and $\Delta^{17}\text{O}$ - NO_3^- (no effect). Measurements located within a mixing range correspond to plant NO_3^- samples containing a mixture of NO_3^- atm and NO_3^- bio. Data points located outside a mixing range correspond to plant NO_3^- samples that were isotopically fractionated (e.g., through assimilation). When significant, the regression lines between sample isotopic values were plotted for leaves (green) and roots (brown). Note that each data point represents the mean value of three plant individuals per sampling date.